Stimulation of P-Glycoprotein ATPase by Analogues of Tetramethylrosamine: Coupling of Drug Binding at the "R" Site to the ATP Hydrolysis Transition State†

Gregory Tombline,*,‡,§ David J. Donnelly,‡ Jason J. Holt,‡ Youngjae You,‡ Mao Ye,‡ Michael K. Gannon,‡ Cara L. Nygren,‡ and Michael R. Detty*,‡

Department of Chemistry, University at Buffalo, The State University of New York, Buffalo, New York 14260-3000, and Department of Biochemistry and Biophysics, University of Rochester Medical Center, 601 Elmwood Avenue, P.O. Box 607, Rochester, New York 14642

Received February 19, 2006; Revised Manuscript Received May 8, 2006

ABSTRACT: The multidrug resistance efflux pump P-glycoprotein (Pgp) couples drug export to ATP binding and hydrolysis. Details regarding drug trajectory, as well as the molecular basis for coupling, remain unknown. Nearly all drugs exported by Pgp have been assayed for competitive behavior with rhodamine123 transport at a canonical "R" drug binding site. Tetramethylrosamine (TMR) displays a relatively high affinity for Pgp when compared to other rhodamines. Here, we present the construction and characterization of a library of compounds based upon the TMR scaffold and use this set to assess the determinants of drug binding to the "R" site of Pgp. This set contained modifications in (1) the number, location, and conformational mobility of hydrogen-bond acceptors; (2) the heteroatom in the xanthylium core; and (3) the size of the substituent in the 9-position of the xanthylium core. Relative specificity for coupling to the distal ATP catalytic site was assessed by ATPase stimulation. We found marked (∼1000-fold) variation in the ATPase specificity constant within the library of TMR analogues. Using established methods involving ADP-Vi trapping by wild-type Pgp and ATP binding by catalytic carboxylate mutant Pgp, these effects can be extended to ATP hydrolysis transition-state stabilization and ATP occlusion at a single site. These data support the idea that drugs trigger the engagement of ATP catalytic site residues necessary for hydrolysis. Further, the nature of the drug binding site and coupling mechanism may be dissected by variation of a drug-like scaffold. These studies may facilitate development of novel competitive inhibitors at the "R" drug site.

P-glycoprotein (Pgp,[1] also known as MDR1 or ABCB1) (*1*−*3*), a mammalian plasma membrane protein, is a member of the ATP-binding cassette (ABC) superfamily and was the first efflux protein identified and associated with multidrug resistance (MDR) in cancer chemotherapy. Pgp is also the most studied of a growing family of proteins known to confer MDR (*3*). Related efflux pumps are associated with resistance in the treatment of AIDS, bacterial, parasitic, and fungal diseases (*4*−*7*). The reversal or inhibition of MDR is a clinically important goal and, numerous classes of compounds have been investigated for this role (*8*, *9*).

Pgp consists of a single polypeptide chain that forms two putative transmembrane domains (TMDs) and two nucleotide-binding domains (NBDs) alternating along the chain. Binding and hydrolysis of ATP at the two NBDs is coupled to drug export via the TMDs. The alternating sites model for the mechanism of Pgp drug export suggested that hydrolysis at a single NBD is sufficient to facilitate a single transport event and that the two NBDs alternatively hydrolyze ATP (*10*). Newer variations of this model suggest that two hydrolysis events are required for each transport cycle (*11*) and that ATP binding (and not hydrolysis) is most important for the primary drug transport event (*12*). ATP hydrolysis and drug transport have been shown to share the same rate-limiting transition state, providing formal proof of coupling of the two and that drugs transported at a higher rate bind the transition state more tightly (*13*). Low-resolution structural analysis has shown that major structural changes occur upon nucleotide binding to Pgp leading to asymmetry in the TMDs (*14*, *15*). Recent structural data of homologues

† This research was supported in part by NIH Grant No. T32 CA09363 (Postdoctoral Training Grant) to G.T. and by the Department of Defense [Breast Cancer Research Program] under Award No. W81XWH-04-1-0708 to M.R.D. and W81XWH-04-1-0368 to D.J.D. Views and opinions of, and endorsements by the author(s), do not reflect those of the U.S. Army or the Department of Defense.

* To whom correspondence should be addressed. For G.T.: current address, Department of Biochemistry and Biophysics, University of Rochester Medical Center, 601 Elmwood Avenue, P.O. Box 607, Rochester, NY 14642; tel., (585)-285-2769; fax, (585)-271-2683; e-mail, Gregory_Tombline@urmc.rochester.edu. For M.R.D.: Tel., (716)-645-6800 x2200; fax, (716)-645-6963; e-mail, mdetty@buffalo.edu.

‡ University at Buffalo, The State University of New York.

§ University of Rochester Medical Center.

[1] Abbreviations: Pgp, P-glycoprotein; MDR, multidrug resistance; ABC, ATP binding cassette; TMR, tetramethylrosamine; TMR-S, thiotetramethylrosamine; TMR-Se, selenotetramethylrosamine; VER, verapamil; R123, rhodamine 123; R6G, rhodamine 6G; TMD, transmembrane domain; NBD, nucleotide binding domain; NCI, National Cancer Institute; ATP, adenosine triphosphate; ADP, adenosine diphosphate; Vi, vanadate anion; Pi, inorganic phosphate; HRMS (EI), high-resolution mass spectrometry (electrospray ionization); THF, tetrahydrofuran; *tert*-BuLi, *tert*-butyllithium; ORTEP, Oak Ridge thermal ellipsoid plot; DMSO, dimethyl sulfoxide; TCEP, tris(2-carboxyethyl)-phosphine hydrochloride; EGTA, ethylene glycol bis-2-aminoethyl ether tetraacetic acid; PEP, phosphoenolpyruvate; DTT, dithiothreitol; CFTR, cystic fibrosis transmembrane conductance regulator.

10.1021/bi0603470 CCC: $33.50
Published on Web 06/08/2006

Chart 1: Structures of Various Rhodamine Dyes and Tetramethylrosamine (TMR)

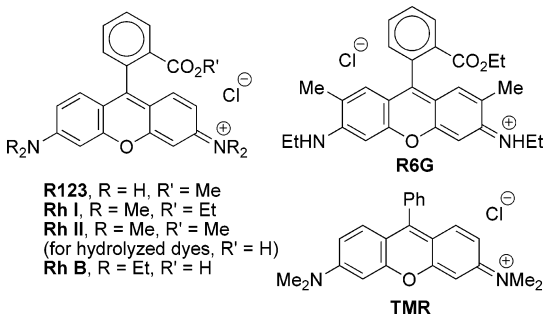

(*16*−*19*), as well as biochemical data with Pgp, indicate that transport results from the formation and collapse of a "closed conformation" in which the NBDs form an interdigitated dimer with ATP bound at two sites (*20*−*24*). Formation and collapse of this intermediate would be governed by ATP binding, hydrolysis, and product release. A key point is that drugs stabilize the closed ATP-bound NBD dimer conformation. In addition, binding of drugs to Pgp appears to elicit asymmetry in the ATP catalytic sites where one becomes tightly bound and poised for hydrolysis (*23*, *24*).

Greater mechanistic understanding will come from studies of drug binding site(s), trajectory of transport, and residues involved in coupling TMD and NBD. This may be challenging since unlike NBDs, which are highly conserved and share catalytic residues with a wide variety of nucleotide binding proteins, the TMDs of ABC transporters are not well-conserved. Transport assays performed using Pgp and fluorescent dyes indicate a minimum of two nonoverlapping binding sites termed "H" and "R" for Hoechest 33342 and Rhodamine 123 (R123, Chart 1), respectively (*25*, *26*). Nontransporting allosteric drug binding sites have also been revealed by these assays. The "H" site has been well-studied and modeled to include many of the effective inhibitors of Pgp (*27*−*29*). Pgp−drug interactions have also been examined by radioligand binding (*30*), electron paramagnetic resonance spectroscopy (*31*), photoaffinity labeling (*32*, *33*), fluorescence spectroscopy (*34*), covalent attachment of MTS-derivatives (thiol-reactive) of drugs to mutants containing a single cysteine (*35*, *36*), and structure−activity studies of compounds that either stimulate ATP hydrolysis or are competitive for transport (*37*). Although structure−activity studies of drug interactions provide reliable biochemical data, they often involve comparison of highly diverse compounds and are limited in that the changes are not systematic; that is, only broad conclusions may be drawn.

Rhodamine dyes have been used as mimics of chemotherapeutic drugs to assay Pgp-mediated transport. Efflux of R123 from cells was used to define Pgp transport substrates/antagonists in a cross-correlation of drug resistance patterns in the NCI 60 set of cells with the NCI Drug Screen Database of compounds (*38*, *39*). Among the rhodamine derivatives of Chart 1, tetramethylrosamine (TMR) has been described as the best transport substrate for Pgp both in viable MDR cells and in reconstituted Pgp (*40*−*42*). In evaluating the transport of this set of rhodamines, the rate constant for outward pumping by Pgp was similar for most of the rhodamines, but was 5- to 10-fold higher for TMR (*42*). Surprisingly, there has been no systematic investigation of analogues of TMR with respect to ATPase stimulation, drug binding, and drug transport. Herein, we have used the library of TMR analogues shown in Chart 2 to probe the binding of TMR analogues to Pgp in order to give insights into the fundamental molecular recognition properties in TMR analogues that allow tight binding to Pgp.

MATERIALS AND METHODS

Materials. All chemicals and reagents were purchased from Sigma Chemical Co. (St. Louis, MO) unless otherwise noted. Elemental analyses were conducted by Atlantic Microlabs, Inc. (Norcross, GA). The compounds TMR-S, TMR-Se, **1**, **2**, **4**, **5**, **9**−**12**, **14**, **15**, **19**, and **20** were prepared from chalcogenoxanthones **23**−**26** (Chart 3) as previously described (*43*, *44*). Xanthone **23** was prepared according to ref *45*. Chalcogenoxanthones **24** and **25** (Chart 3) were prepared according to ref *46*. Thioxanthone **26** was prepared according to ref *47*.

*Synthesis of 3,6-Bis(dimethylamino)-9-(3-methoxyphenyl)-xanthylium Hexafluorophosphate (**3**).* A mixture of 1-bromo-3-methylbenzene (1.53 g, 8.0 mmol) and ground magnesium turnings (0.34 g, 14 mmol) in 8 mL of anhydrous THF was heated at reflux for 1 h and then cooled to ambient temperature. The resulting solution of Grignard reagent was then added to a solution of 3,6-bis(dimethylamino)-9-xanthenone (**23**, 0.10 g, 0.40 mmol) in anhydrous THF (3 mL). The reaction mixture was heated at reflux for 1 h and cooled to ambient temperature and then to 0 °C. Then, acetic acid (0.5 mL) was added. Hexafluorophosphoric acid (10% by-weight solution in water, 25 mL) was added dropwise until a color change (blue to yellow) was observed. The resulting solution was poured into ice water (200 mL), and the resulting solid was recrystallized from CH_3CN/ether to give 0.100 g (55%) of **3** as a green crystalline solid, mp > 260 °C; ^{1}H NMR (500 MHz, CD_2Cl_2): δ 7.60 (d×d, 1 H, J = 7.5, 8.5 Hz), 7.48 (d, 2 H, J = 9.6 Hz), 7.23 (d×d×d, 1 H, J = 1.0, 1.5, 8.5 Hz), 7.02 (d×d×d, 1 H, J = 1.0, 1.5, 7.5 Hz), 6.98 (m, 1 H), 6.96 (m, 2 H), 6.86 (d, 2 H, J = 2.7 Hz), 3.91 (s, 3 H), 3.34 (s, 12 H); ^{13}C NMR (125 MHz, $CDCl_3$): δ 159.6, 159.0, 134.7, 133.5, 131.8, 123.3, 117.2, 116.9, 115.7, 115.1, 98.1, 57.1, 42.4; λ_{max} (H_2O) 552 nm (ϵ 1.2 × 10^5 M^{-1} cm^{-1}); high-resolution mass spectrometry (electrospray ionization) [HRMS (EI)] *m*/*z* 373.1900 (calcd for $C_{24}H_{25}N_2O_2$: 373.1911). Anal. Calcd for $C_{24}H_{25}N_2O_2PF_6$: C, 55.60; H, 4.86; N 5.40. Found: C, 55.75; H, 5.10; N, 5.37.

*Synthesis of 3,6-Bis(dimethylamino)-9-(3,4-dimethoxyphenyl)xanthylium Hexafluorophosphate (**6**).* 1-Bromo-3,4-dimethoxybenzene (2.11 g, 9.74 mmol), ground magnesium turnings (0.22 g, 8.86 mmol), and 3,6-bis(dimethylamino)-9-xanthenone (**23**, 0.25 g, 0.89 mmol) in 10 mL of anhydrous THF were treated as described for the preparation of **3**. Product yield was 0.32 g (66%) of **6** as a dark red solid, mp > 260 °C; ^{1}H NMR (500 MHz, CD_2Cl_2): δ 7.58 (d, 2 H, J = 9.5 Hz), 7.16 (d, 1 H, J = 8.5 Hz), 7.04 (d×d, 1 H, J = 1.5, 8.0 Hz), 6.99 (d×d, 2 H, J = 2.5 Hz), 6.97 (d×d, 2 H, J = 2.5, 8.5 Hz), 6.85 (d, 1 H, J = 2 Hz), 4.01 (s, 3 H), 3.90 (s, 3 H), 3.34 (s, 12 H); ^{13}C NMR (125 MHz, CD_2Cl_2): δ 158.7, 157.9, 157.2, 151.2, 149.4, 132.1, 123.8, 123.0, 114.0, 113.6, 113.0, 111.5, 96.4, 56.1, 56.0, 40.7; λ_{max} (H_2O) 520 (ϵ 3.95 × 10^4 M^{-1} cm^{-1}), 550 nm (ϵ 8.51 × 10^4 M^{-1}

Chart 2: Library of Chalcogenoxanthylium Analogues of TMR and Their Xanthone Precursors

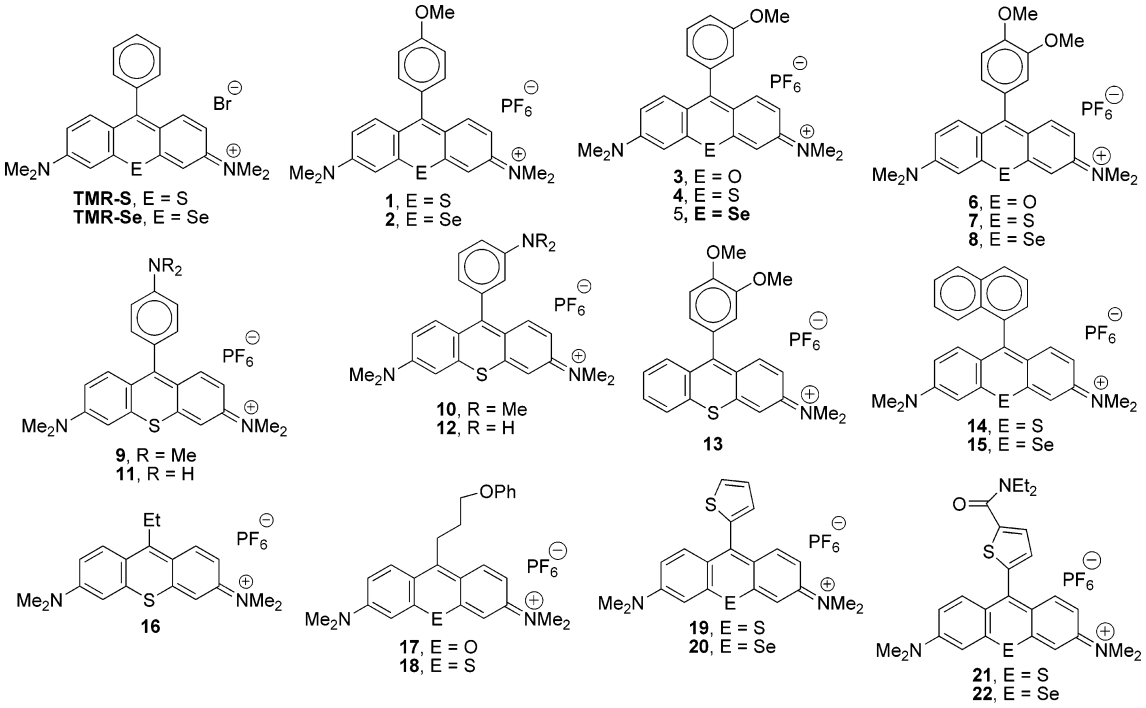

Chart 3: Chalcogenoxanthone Precursors to TMR Analogues

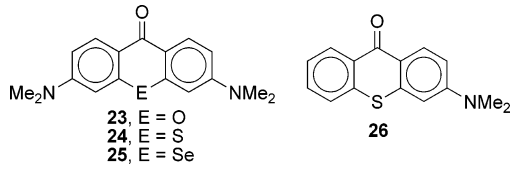

cm^{-1}). HRMS (EI) *m*/*z* 403.2012 (calcd for $C_{25}H_{27}N_2O_3$: 403.2016). Anal. Calcd for $C_{25}H_{27}F_6N_2O_3P$: C, 54.75; H, 4.96; N, 5.11. Found: C, 54.31; H, 4.75; N, 5.11.

*Synthesis of 3,6-Bis(dimethylamino)-9-(3,4-dimethoxyphenyl)thioxanthylium Hexafluoro-phosphate (**7**).* 1-Bromo-3,4-dimethylbenzene (1.8 g, 8.0 mmol), ground magnesium turnings (0.20 g, 8.1 mmol), and 3,6-bis(dimethylamino)-9-thioxanthenone (**26**, 0.20 g, 0.67 mmol) in 10 mL of anhydrous THF were treated as described for the preparation of **3**. Product yield was 0.323 g (85%) of **7** as a green crystalline solid, mp 255−256 °C; ^{1}H NMR (500 MHz, CD_2Cl_2): δ 7.56 (d, 2 H, J = 9.5 Hz), 7.09 (m, 3 H), 6.94 (d×d, 2 H, J = 2.5, 8.5 Hz), 6.88 (d×d, 1 H, J = 2.0, 8 Hz), 6.82 (d, 1 H, J = 2.0 Hz), 3.97 (s, 3 H), 3.83 (s, 3 H), 3.28 (s, 12 H); ^{13}C NMR (125 MHz, $CDCl_3$): δ 161.3, 154.0, 150.8, 149.8, 145.0, 137.4, 128.1, 122.7, 120.0, 115.7, 113.4, 111.9, 105.9, 56.6, 41.1; λ_{max} (H_2O) 576 nm (ϵ 7.5 × 10^4 M^{-1} cm^{-1}); HRMS (EI) *m*/*z* 419.1787 (calcd for $C_{25}H_{27}N_2O_2S$: 419.1788). Anal. Calcd for $C_{25}H_{27}N_2O_2SPF_6$: C, 53.19; H, 4.82; N, 4.96. Found: C, 53.02; H, 4.71; N, 5.14.

*Synthesis of 3,6-Bis(dimethylamino)-9-(3,4-dimethoxyphenyl)selenoxanthylium Hexafluoro-phosphate (**8**).* A mixture of 1-bromo-3,4-dimethylbenzene (1.8 g, 8.0 mmol), ground magnesium turnings (0.20 g, 8.1 mmol), and 3,6-bis-(dimethylamino)-9-selenoxanthenone (**25**, 0.10 g, 0.40 mmol) in 10 mL of anhydrous THF was treated as described for the preparation of **3**. Product yield was 0.100 g (43%) of **8** as a green crystalline solid, mp 255−256 °C: ^{1}H NMR (500 MHz, CD_2Cl_2): δ 7.68 (d, 2 H, J = 2.8 Hz), 7.57 (d, 2 H, J = 9.8 Hz), 7.22 (d, 1 H, J = 8.2 Hz), 7.11 (d×d, 2 H, J = 2.8, 9.8 Hz), 7.04 (d, 1 H, J = 2.2 Hz), 6.92 (d×d, 1 H, J = 2.2, 8.2 Hz), 3.96 (s, 3 H), 3.84 (s, 3 H), 3.56 (s, 12 H); ^{13}C NMR (125 MHz, $CDCl_3$): δ 161.8, 152.9, 149.7, 148.9, 146.1, 138.6, 128.9, 121.9, 120.1, 114.7, 112.5, 111.1, 108.8, 56.1, 56.0, 40.5; λ_{max} (H_2O) 580 nm (ϵ 1.01 × 10^5 M^{-1} cm^{-1}); HRMS (EI) *m*/*z* 467.1233 (calcd for $C_{25}H_{27}N_2O_2{}^{80}$Se: 467.1232). Anal. Calcd for $C_{25}H_{27}N_2O_2SePF_6$: C, 49.11; H, 4.45; N, 4.58. Found: C, 48.97; H, 4.46; N, 4.58.

*Synthesis of 3-Dimethylamino-9-(3,4-dimethoxyphenyl)-thioxanthylium Hexafluorophosphate (**13**).* A mixture of 1-bromo-3,4-dimethylbenzene (1.8 g, 8.0 mmol), ground magnesium turnings (0.20 g, 8.1 mmol), and 3-(dimethylamino)-9-thioxanthenone (**26**, 0.10 g, 0.40 mmol) in 10 mL of anhydrous THF was treated as described for the preparation of **3**. Product yield was 0.050 g (25%) of **13** as a green crystalline solid, mp 250−251 °C; ^{1}H NMR (500 MHz, CD_2Cl_2): δ 8.03 (d×d, 1 H, J = 0.6, 8.2 Hz), 7.84 (m, 3 H), 7.59 (d×d×d, 1 H, J = 1.0, 1.5, 8.2 Hz), 7.35 (d, 1 H, J = 2.7 Hz), 7.22 (d×d, 1 H, J = 2.7, 10.0 Hz), 7.13 (d, 1 H, J = 8.2 Hz), 6.93 (d×d, 1 H, J = 1.8, 7.9 Hz), 6.87 (d, 1 H, J = 1.8 Hz), 3.99 (s, 3 H), 3.84 (s, 3 H), 3.44 (s, 6 H); ^{13}C NMR (75 MHz, CD_2Cl_2): δ 156.0, 150.3, 150.0, 140.1, 136.2, 135.4, 130.6, 129.9, 128.4, 127.6, 124.8, 124.2, 120.5, 114.7, 113.2, 107.7, 57.7, 57.6, 43.3 (3 overlapped peaks); λ_{max} (H_2O) 562 nm (ϵ 6.5 × 10^4 M^{-1} cm^{-1}); HRMS (EI) *m*/*z* 376.1365 (calcd for $C_{23}H_{22}NO_2S$: 376.1366). Anal. Calcd for $C_{23}H_{22}NO_2SPF_6$: C, 52.98; H, 4.25; N, 2.69. Found: C, 53.33; H, 4.39; N, 2.44.

*Synthesis of 3,6-Bis(dimethylamino)-9-ethylthioxanthylium Hexafluorophosphate (**16**).* Ethylmagnesium bromide (2.1 mL of a 1.0 M solution in ether, 2.1 mmol) was added dropwise to a solution of **24** (0.16 g, 0.53 mmol) in anhydrous THF (10 mL). The resulting mixture was heated at reflux for 2 h, cooled to ambient temperature, and poured into acetic acid (3.0 mL). Hexafluorophosphoric acid (60%

weight solution in water) was added dropwise until a color change was observed. Water (50 mL) was added, and the solution was cooled to −10 °C. The resulting precipitate was collected by filtration, and the solid was washed with water (10 mL) and diethyl ether (10 mL). The crude product was recrystallized from CH_3CN and a small amount of ether to give 0.13 g (71%) of **16** as a green crystalline solid, mp > 260 °C; ^{1}H NMR (500 MHz, CD_3OD): δ 8.33 (d, 2 H, J = 9.5 Hz), 7.20 (d×d, 2 H, J = 2.0, 9.5 Hz), 7.15 (d, 2 H, J = 2.0 Hz), 3.52 (q, 2 H, J = 7.0 Hz), 3.21 (s, 12 H), 1.35 (t, 3 H, J = 7.0 Hz); λ_{max} (H_2O) 565 nm (ϵ 7.1 × 10^4 M^{-1} cm^{-1}); HRMS (EI) *m*/*z* 311.1575 (calcd for $C_{19}H_{23}N_2S$: 311.1576). Anal. Calcd for $C_{19}H_{23}N_2SPF_6$: C, 50.00; H, 5.08; N, 6.14. Found: C, 50.03; H, 4.99; N, 5.98.

*Synthesis of 3,6-Bis(dimethylamino)-9-(3-phenoxypropyl)-xanthylium Hexafluorophosphate (**17**).* A mixture of 3-phenoxypropyl bromide (0.84 g, 3.90 mmol) and ground magnesium turnings (0.10 g, 4.25 mmol) in 4 mL of anhydrous THF was heated at reflux for 0.5 h and then cooled to ambient temperature. The resulting solution was added to 3,6-bis(dimethylamino)-9-xanthenone (**23**, 0.10 g, 0.35 mmol) in anhydrous THF (2 mL). The reaction mixture was heated at reflux for 0.5 h and cooled to ambient temperature and then to 0 °C. Acetic acid (0.5 mL) was added. Hexafluorophosphoric acid (10% by-weight solution in water, 10 mL) was added dropwise until a color change was observed. The resulting solution was poured into ice water (200 mL), and the crude product was collected by filtration. The crude product was purified via chromatography on SiO_2 eluted with MeOH/EtOAc/CH_2Cl_2 (1:2:7). The pink fractions were collected and recrystallized from ethyl acetate to yield 20 mg (10%) of **17** as a dark red solid, mp > 260 °C; ^{1}H NMR (400 MHz, CD_2Cl_2): δ 8.06 (d, 2 H, J = 9.6 Hz), 7.35 (t, 2 H, J = 8.0 Hz), 7.00−7.09 (m, 3 H), 6.95 (d, 2 H, J = 8.0 Hz), 6.78 (d, 2 H, J = 2 Hz), 4.12 (t, 2 H, J = 6 Hz), 3.60 (t, 2 H, J = 7 Hz), 3.33 (s, 12 H), 2.31 (quint, 2 H, J = 7 Hz); λ_{max} (H_2O) 542 nm (ϵ 1.14 × 10^5 M^{-1} cm^{-1}); HRMS (EI) *m*/*z* 401.2237 (calcd for $C_{26}H_{29}N_2O_2$: 401.2224). Anal. Calcd for $C_{26}H_{29}N_2O_2(H_2O)_{0.25}$: C, 56.68; H, 5.40; N, 5.08. Found: C, 56.68; H, 5.42; N, 5.09. The 0.25 water of hydration integrates appropriately in the ^{1}H NMR spectrum of **17** relative to the background water in $CDCl_3$.

*Synthesis of 3,6-Bis(dimethylamino)-9-(3-phenoxypropyl)-thioxanthylium Hexafluorophosphate (**18**).* 3-Phenoxypropyl bromide (2.16 g, 10.1 mmol), ground magnesium turnings (0.33 g, 13.4 mmol), and thioxanthenone **24** (0.20 g, 0.67 mmol) in 50 mL of anhydrous THF were treated as described for the preparation of **17**. Product yield was 0.088 g (23%) of **18** as a dark red solid, mp > 260 °C; ^{1}H NMR (400 MHz, CD_2Cl_2): δ 8.35 (d, 2 H, J = 9.6 Hz), 7.32 (t, 2 H, J = 8.0 Hz), 7.09 (d×d, 2 H, J = 2.8, 9.6), 7.02 (d, 2 H, J = 2.8 Hz), 6.978 (t, 3 H, J = 8 Hz), 4.14 (t, 2 H, J = 7 Hz), 3.70 (t, 2 H, J = 8 Hz), 3.28 (s, 12 H), 2.27 (quint, 2 H, J = 7 Hz); ^{13}C NMR (125 MHz, $CDCl_3$): δ 162.2, 159.1, 153.8, 144.7, 133.8, 130.1, 121.6, 119.2, 116.4, 115.0, 105.9, 66.9, 41.0, 31.9, 30.2; HRMS (EI) *m*/*z* 417.2001 (calcd for $C_{26}H_{29}N_2OS$: 417.1995); λ_{max} (H_2O) 542 nm (ϵ 1.14 × 10^5 M^{-1} cm^{-1}).

*Synthesis of 3,6-Bis(dimethylamino)-9-(N,N-*diethyl-5-thiophene-2-carboxamide)selenoxanthyliu*m Hexafluorophosphate (**22**). 1. Preparation of 5-Bromo-N,N-diethylthiophene-2-carboxamide (**27**).* Thionyl chloride (1.1 mL, 15 mmol) was added to a stirred solution of 5-bromo-2-thiophenecarboxylic acid (1.0 g, 4.8 mmol) in 25 mL CH_2Cl_2 at 0 °C. Diethylamine (3.0 mL, 29 mmol) was added dropwise, and the resulting mixture was stirred for 0.5 h at 0 °C, warmed to room temperature, and stirred for 1 h. The reaction was slowly quenched with saturated $NaHCO_3$ (100 mL). The CH_2Cl_2 layer was separated, and the aqueous layer was extracted with CH_2Cl_2 (2 × 50 mL). The combined organic extracts were washed with brine, dried over $MgSO_4$, and concentrated. The resulting yellow oil was purified via chromatography on SiO_2 eluted with 2:1 EtOAc−hexanes (R_f = 0.8) to give 1.0 g (75%) of the amide **27** as a clear oil. IR (NaCl plate); ^{1}H NMR (500 MHz, $CDCl_3$): δ 7.07 (d, 1 H, J = 4.0 Hz), 6.97 (d, 1 H, J = 4.0 Hz), 3.51 (q, 4 H, J = 7.0 Hz), 1.23 (t, 6 H, J = 7.0 Hz); ^{13}C NMR (126 MHz, $CDCl_3$): δ 199.5, 129.7, 128.5, 128.4, 33.7, 27.7. HRMS (EI) *m*/*z* 260.9817 (calcd for $C_9H_{12}NOS^{79}Br$: 260.9823). Anal. Calcd for $C_9H_{12}BrNOS$: C, 41.23; H, 4.61; N, 5.34. Found: C, 41.41; H, 4.64; N, 5.30.

2. Addition of N,N-Diethyl 2-Lithio-5-thiophenecarboxamide. A solution of *tert*-butyllithium (*tert*-BuLi, 4.5 mL of a 1.6 M solution, 7.2 mmol) was added dropwise to 5-bromo-*N*,*N*-diethylthiophene-2-carboxamide (**27**, 0.90 g, 3.5 mmol) dissolved in freshly distilled anhydrous THF (5.0 mL) cooled to −78 °C. After 1 min, the resulting solution was added via cannula to a solution of 3,6-bis(dimethylamino)-9-selenoxanthenone (**25**, 0.173 g, 0.50 mmol) in THF (10 mL) at −78 °C. After 5 min, the reaction mixture was poured into acetic acid (3.0 mL). HPF_6 (60% weight solution in water) was added dropwise until a color change (blue to gold) was observed. Water (50 mL) was added, and the solution was cooled to −10 °C. The resulting mixture was extracted with CH_2Cl_2 (3 × 100 mL) and concentrated. The crude product was purified by chromatography on SiO_2 eluted first with MeOH/EtOAc/CH_2Cl_2 (1:2:7) to separate unreacted **27** from the dye mixture. The chromatography was then repeated eluting with MeOH/EtOAc/CH_2Cl_2 (1:2:7) to separate three distinct dye bands. The desired product was the low Rf band. The upper two dye bands were identified as containing multiple thiophene units from self-condensation of the 5-lithio-2-thiophenecarboxamide. The desired product band was recrystallized from acetonitrile/EtOAc to give **22** as dark purple needles (0.034 g, 11%), mp > 260 °C; ^{1}H NMR (400 MHz, CD_2Cl_2): δ 7.72 (d, 2 H, J = 2.2 Hz), 7.70 (d, 2 H, J = 9.8 Hz), 7.49 (d, 1 H, J = 3.7 Hz), 7.17 (d, 1 H, J = 3.7 Hz), 6.94 (d×d, 2 H, J = 2.2, 9.8 Hz), 3.65 (s, broad, 4 H), 3.33 (s, 12 H), 1.39 (s, broad, 6 H); λ_{max} (H_2O) 597 nm (ϵ 8.0 × 10^4 M^{-1} cm^{-1}), HRMS (EI) *m*/*z* 512.1268 (calcd for $C_{26}H_{30}N_3OS^{80}Se$: 512.1269).

*Synthesis of 3,6-Bis(dimethylamino)-9-(N,N-diethyl-5-thiophene-2-carboxamide)thioxanthylium Hexafluorophosphate (**21**).* 5-Bromo-*N*,*N*-diethylthiophene-2-carboxamide (**27**, 0.70 g, 2.7 mmol), 3,6-bis(dimethylamino)-9-thioxanthenone (**24**, 0.150 g, 0.50 mmol), and 0.97 M *tert*-BuLi (5.6 mL, 5.4 mmol) in freshly distilled anhydrous THF (10 mL) were treated as described for the preparation of **22** to give 0.027 g (11%) of **21** as a green crystalline solid, mp > 260 °C; ^{1}H NMR (400 MHz, CD_2Cl_2): δ 7.68 (d, 2 H, J = 9.6 Hz), 7.46 (d, 1 H, J = 3.6 Hz), 7.15 (d, 1 H, J = 3.6 Hz), 7.06 (d, 2 H, J = 2.4 Hz), 6.98 (d×d, 2 H, J = 2.4, 9.6 Hz), 3.60 (s, broad, 4 H), 3.28 (s, broad, 12 H), 1.39 (s, broad, 6 H); λ_{max} (H_2O) 594 nm (ϵ 8.0 × 10^4 M^{-1} cm^{-1});

HRMS (EI) *m/z* 464.1836 (calcd for $C_{26}H_{30}N_3OS_2$: 464.1825).

Determination of n-Octanol/Water Partition Coefficients. The octanol/water partition coefficients were all measured at pH 6 (phosphate-buffered) using UV−vis spectrophotometry. The measurements were done using a 'shake flask' direct measurement (*48*). Mixing for 3−5 min was followed by 1 h of settling time. Equilibration and measurements were made at 23 °C using a Perkin-Elmer Lambda 12 spectrophotometer.

X-ray Diffraction Data. X-ray diffraction data on TMR-S and TMR-Se were collected at 90(1) K using a Bruker SMART APEX2 CCD diffractometer installed at a rotating anode source (Mo Kα radiation, $\lambda = 0.71073$ Å), and equipped with an Oxford Cryosystems nitrogen gas-flow apparatus. The data were collected by the rotation method with 0.3° frame-width (ω scan) and 20 s exposure time per frame. Four sets of data (600 frames in each set) were collected for each compound, nominally covering complete reciprocal space. The data were integrated, scaled, sorted, and averaged using the SMART software package (*49*). The structure was solved by direct methods using SHELXTL NT Version 6.14 (*50*). The structure was refined by full-matrix least squares against F^2.

Non-hydrogen atoms were refined anisotropically. Positions of hydrogen atoms were found by difference electron density Fourier synthesis. The CH_3 hydrogens were treated as part of idealized CH_3 groups with $U_{iso} = 1.5U_{eq}$, while the remainder of the hydrogen atoms were refined with the "riding" model with $U_{iso} = 1.2U_{eq}$.

Crystallographic data are compiled in Table 1S in Supporting Information. Atomic coordinates, anisotropic displacement parameters, bond lengths, and angles are given in Tables 2S−4S, respectively, for TMR-S and Tables 5S−7S, respectively, for TMR-Se, in Supporting Information.

Expression, Purification, Quantitation, and Activation of Pgp. Strains of yeast *Pichia pastoris* expressing mouse MDR3 wild-type or Cys-less Pgp were grown in fermentor culture and purified as described (*23*, *51*). We note that Mouse MDR3 Pgp is 87% identical to human MDR1 Pgp in sequence (*51*). Pgp concentration was determined by quantitation after SDS-gel electrophoresis on 10% gels and Coomassie Blue staining. Several dilutions of unknown Pgp were resolved alongside a similar series of a reference preparation whose concentration had previously been accurately determined by amino acid analysis. Protein bands were quantified with Scion Image software (Scion Corporation, Frederick, MD). Pgp was stored in aliquots at −70 °C with excellent retention of activity. Just prior to each experiment, Pgp was activated by incubation with a 2:1 (w/w) equivalent of *Escherichia coli* lipids (Avanti; acetone/ether-precipitated) for 20 min at room temperature followed by sonication for 30 s at 4 °C in a bath sonicator. For wild-type protein, 10 mM TCEP (Tris(2-carboxyethyl)phosphine hydrochloride) was included during the 20-min incubation in order to reduce the inhibitory disulfide between P-loop cysteines.

ATPase Assays. ATP hydrolysis was determined by the spectrophotometric-coupled assay performed in microplate format in 96-well plates (*51*). Each reaction contained 5 μg of lipid-activated Cys-less MDR3 Pgp with the indicated amount of VER, Rh 123, R6G, or TMR analogue added in 1-μL volume from concentrated DMSO stock solutions. Cys-less protein was chosen for the initial ATPase screening due to the fact that it displays wild-type ATPase activity (*37*), and DTT, which is necessary to activate wild-type Pgp, was found to reduce some of the compounds. DMSO was 2% final concentration in all reactions. Each 50-μL reaction contained 40 mM Tris-HCl, pH 7.4, 0.1 mM EGTA, 10 mM NaATP, 12 mM $MgSO_4$, 3 mM PEP, 1.5 mM NADH, and pyruvate kinase and lactate hydrogenase (each at a final concentration of 0.1 mg/mL). Reactions were kept on ice and in the dark until placed in the plate reader. Kinetics of NADH oxidation was followed at 37 °C by a decrease in absorption at 340 nm, and this was converted into a specific activity for moles ATP hydrolyzed. Control reactions containing DMSO alone or 150 μM VER were performed in parallel for comparison. Assays were performed in a Spectramax Gemini Plate reader and analyzed with SOFTmaxPro software. Initial stimulation of ATPase activity for drug titrations were fitted with an activity-partitioning model as described earlier (*13*, *52*) using SigmaPlot 2000 software. In this model, P-glycoprotein partitions its activity between an uncoupled basal activity cycle or a coupled activity cycle depending on drug concentration. The steady-state ATPase activity was fitted by the following equation:

$$v = \{V_B + ((V_M - V_B)[\text{drug}]/(K_M^D + [\text{drug}]))\}\{1 - ([\text{drug}]/(K_i + [\text{drug}]))\} \quad (1)$$

where, V is the ATPase activity, [drug] is the concentration of VER, Rh 123, R6G, or TMR analogue, V_B is the maximal basal ATPase activity (apparent V_{max}) in the absence of drug, V_M is the maximal drug-stimulated ATPase activity (apparent V_{max}) in the presence of drug, K_M^D is the Michaelis constant for drug activation, and K_i is the inhibition constant for drug inhibition (see below).

At higher concentrations, drug-stimulated Pgp ATPase activity can be inhibited by binding of the drug to a second allosteric site (*13*, *52*). However, solubility limitations prevented drug titration curves at concentrations approaching millimolar or higher. Consequently, inhibition was not observed at the highest concentrations of drug employed in these studies, K_i was assumed to be > 1000 μM in these studies, and eq 1 reduces to

$$v = V_B + ((V_M - V_B)[\text{drug}]/(K_M^D + [\text{drug}])) \quad (2)$$

The kinetic constants K_M^D, V_B, and V_M were obtained by fitting drug titration data with this equation using SigmaPlot 2000 software, and data are compiled in Table 1.

The maximal drug-induced ATPase activity, V_M^{ATP}, is reported in two ways in Table 1: as a specific activity in units of (nmol/min)/μg of protein and as a molar turnover number based on Cys-less MDR3 Pgp as a nonglycosylated 140 kDa protein. The latter value has the dimensions of (mol ATP/s)/mol Pgp or s^{-1}. The molar turnover number for V_M^{ATP} was used to give the catalytic rate constant for each drug with

$$k_a(\text{ATPase}) = V_M^{ATP}/K_M^D \quad (3)$$

in units of M^{-1} s^{-1}. Unitless comparisons of values of k_a(ATPase) are given as values of k_{rel} in Table 1.

Table 1: Maximal ATPase Activity (V_M^{ATP}), Associated Values of K_M^D, and Catalytic Rate Constant [k_a(ATPase)] for VER, R123, R6G, TMR, TMR-S, TMR-Se, and **1**−**22**[a]

compd	log *P*	slope V_M	K_M^D, μM	V_M^{ATP}, (nmol/min)/μg	V_M^{ATP}, s^{-1} ((mol/s)/mol)	k_a(ATPase), $M^{-1}\,s^{-1}$	k_{rel}
basal	-	12 ± 2	ND[b]	0.40 ± 0.07	0.94 ± 0.16	-	-
VER	5.1	125 ± 3	20 ± 4	4.17 ± 0.10	9.78 ± 0.23	4.9×10^5	6.4
R123	1.06 ± 0.06	87 ± 15	231 ± 111	2.90 ± 0.50	6.81 ± 1.17	0.29×10^5	0.4
R6G	2.37 ± 0.02	103 ± 6	26 ± 8	3.43 ± 0.20	8.06 ± 0.47	3.10×10^5	4.0
TMR	0.05 ± 0.02	64 ± 3	64 ± 13	2.13 ± 0.10	5.01 ± 0.23	0.78×10^5	1.0
TMR-S	0.07 ± 0.02	68 ± 3	70 ± 15	2.27 ± 0.10	5.32 ± 0.23	0.76×10^5	1.0
TMR-Se	−0.09 ± 0.09	28 ± 6	74 ± 19	0.93 ± 0.20	2.19 ± 0.47	0.30×10^5	0.4
1	−0.09 ± 0.02	55 ± 3	78 ± 22	1.83 ± 0.10	4.30 ± 0.23	0.55×10^5	0.7
2	0.18 ± 0.09	48 ± 5	70 ± 30	1.60 ± 0.17	3.76 ± 0.39	0.54×10^5	0.7
3	0.08 ± 0.01	64 ± 6	7 ± 4	2.13 ± 0.20	5.01 ± 0.47	7.2×10^5	9.1
4	0.14 ± 0.01	68 ± 2	20 ±3	2.27 ± 0.07	5.32 ± 0.16	2.7×10^5	3.4
5	0.20 ± 0.03	74 ± 3	28 ± 6	2.47 ± 0.10	5.79 ± 0.23	2.1×10^5	2.6
6	0.62 ± 0.03	97 ± 4	54 ± 9	3.23 ± 0.13	7.59 ± 0.31	1.4×10^5	1.7
7	0.28 ± 0.05	59 ± 2	26 ± 6	1.97 ± 0.07	4.62 ± 0.16	1.8×10^5	2.2
8	0.18 ± 0.05	45 ± 2	36 ± 10	1.50 ± 0.07	3.52 ± 0.16	0.98×10^5	1.3
9	0.94 ± 0.01	54 ± 12	392 ± 219	1.80 ± 0.40	4.23 ± 0.94	0.11×10^5	0.1
10	1.13 ± 0.02	58 ± 5	131 ± 52	1.93 ± 0.17	4.54 ± 0.39	0.35×10^5	0.4
11	0.20 ± 0.02	45 ± 2	20 ± 6	1.50 ± 0.07	3.52 ± 0.16	1.8×10^5	2.2
12	0.05 ± 0.02	58 ± 8	18 ± 14	1.93 ± 0.27	4.54 ± 0.63	2.5×10^5	3.3
13	0.62 ± 0.03	16 ± 2	ND[b]	0.53 ± 0.07	1.25 ± 0.16	-	-
14	1.80 ± 0.05	25 ± 2	68 ± 24	0.83 ± 0.07	1.96 ± 0.16	0.29×10^5	0.4
15	1.80 ± 0.05	11 ± 2	ND[b]	0.37 ± 0.07	0.86 ± 0.16	-	-
16	0.05 ± 0.02	108 ± 5	54 ± 40	3.60 ± 0.17	8.45 ± 0.39	1.6×10^5	2.1
17	2.20 ± 0.05	59 ± 3	30 ± 8	1.97 ± 0.17	4.62 ± 0.23	1.5×10^5	2.1
18	2.15 ± 0.05	78 ± 5	9 ± 3	2.60 ± 0.10	6.10 ± 0.39	6.8×10^5	8.8
19	−0.49 ± 0.03	12 ± 4	ND[b]	0.40 ± 0.13	0.94 ± 0.31	-	-
20	−0.31 ± 0.04	28 ± 2	30 ±23	0.93 ± 0.07	2.19 ± 0.16	0.73×10^5	0.9
21	−0.39 ± 0.08	120 ± 4	4 ± 1	4.00 ± 0.13	9.39 ± 0.31	23.5×10^5	30.2
22	−0.39 ± 0.08	151 ± 8	6 ± 1	5.03 ± 0.27	11.82 ± 0.63	19.7×10^5	25.3

[a] All values ± standard deviation. [b] ND, not determined.

ADP·Vi Trapping. Drug stimulation of ADP·Vi trapping in the absence of hydrolysis was performed as described in ref *20*. This method relies on the measurement of residual ATPase activity to detect stoichiometry of ADP·Vi trapping (inhibited form). In this approach, an initial inhibited fraction of Pgp exists as a Pgp·ADP·Vi complex in the absence of drug. Drug enhancement is detected as an increase in the fraction of Pgp·ADP·Vi inhibited complex. Briefly, 10 μg of lipid-activated wild-type Pgp was incubated in a 50-μL volume with 40 mM TrisHCl, pH7.4, 0.1 mM EGTA, 100 μM ADP, 2.1 mM $MgSO_4$, 200 μM Vi, and the indicated amount of drug added from concentrated DMSO stocks. In all cases, DMSO was 2% final concentration. Samples were incubated in polypropylene 96-well microplates wrapped in aluminum foil for 2 h at 37 °C and then placed on ice for 10 min. Next, 50 μL of ice-cold TE buffer (40 mM TrisHCl, pH 7.4, 0.1 mM EGTA) was added, and the samples were passed through centrifuge columns to remove free ADP, Vi, and drug. Next, residual ATPase was determined for the eluted samples by the microplate method described above with 150 μM VER added to all samples. All samples were handled in the dark in order to prevent photoinactivation of Pgp by some of the TMR derivatives. Loss of ATPase activity as a function of drug concentration was fit to an equation with a single exponential using SigmaPlot 2000 software.

Drug stimulation of ADP·Vi trapping after hydrolysis (and release of phosphate) was performed as described (*20*, *23*, *24*). This method relies on the measurement of [α-^{32}P]ADP·Vi complex retained by Pgp after passage through a centrifuge column containing G-50 sephadex. Drug enhancement is detected as an increase in the fraction of Pgp·ADP·Vi inhibited complex. Briefly, 10 μg of lipid- and DTT-activated wild-type Pgp was incubated in a 50-μL volume with 40 mM TrisHCl, pH7.4, 0.1 mM EGTA, 200 μM [α-^{32}P]ATP, 2.2 mM $MgSO_4$, 200 μM Vi, and the indicated amount of drug added from concentrated DMSO stocks. In all cases, DMSO was 2% final concentration. Samples were incubated for 10 min at 37 °C and then placed on ice for 10 min. All manipulations were performed in the dark. Next, 50 μL of ice-cold TE buffer (40 mM TrisHCl, pH 7.4, 0.1mM EGTA) was added, and the samples were passed through centrifuge columns. Retained [α-^{32}P]ADP·Vi complex was quantitated by Cerenkov counting.

ATP Occlusion Assay. Drug stimulation of ATP occlusion by E552A/E1197A double "catalytic carboxylate" mutant Pgp was performed as described (*23*, *24*). Similar to the [α-^{32}P]ADP·Vi trapping studies above, this method relies on the measurement of [α-^{32}P]ATP retained by E552A/E1197A Pgp after passage through a centrifuge column containing G-50 sephadex. Assays were identical to above, except that Vi was omitted, and 10 μg of E552A/E1197A Pgp replaced wild-type Pgp.

RESULTS

Library of TMR-Related Structures. The basic scaffold for TMR derivatives and the numbering scheme used in describing the structures is shown in Chart 4. We prepared the focused library of TMR-related structures shown in Chart 2 which includes thioxanthylium (TMR-S) and selenoxanthylium (TMR-Se) analogues of TMR as well as derivatives **1**−**22** bearing a variety of different substituents in the 9-position. This library was designed to examine the effect

Chart 4: Numbering Sequence in the TMR Scaffold

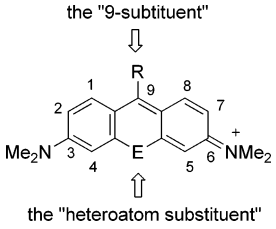

of single-substituent changes in the TMR scaffold including the following: (1) heteroatom substitution in the xanthylium core; (2) the impact of the number and placement of hydrogen-bond donors and acceptors in substituents at the 9-position; and (3) the size limitations of substituents at the 9-postion on ATPase activity in lipid-activated mouse MDR3 Cys-less Pgp (*51*). TMR, TMR-S, and TMR-Se and derivatives **1**−**22** have no ionizable groups and, consequently, always bear a formal positive charge at physiological pH. Experimental values of the *n*-octanol/water partition coefficient, log *P*, were measured for each of these derivatives and are compiled in Table 1. The majority of values of log *P* fall in the −0.5−1.0 range with the 9-dimethylaminophenyl derivative **10**, the 9-(1-naphthyl) derivatives **14** and **15**, and the phenoxypropyl derivatives **17** and **18** representing more hydrophobic derivatives outside this range (log *P* of 1.13, 1.80, 1.80, 2.20, and 2.15, respectively.) Values of log *P* in Table 1 for R123 (1.06) and R6G (2.37) were taken from the literature (*54*). The value of log *P* in Table 1 for verapamil was calculated (*55*). All of the compounds in Chart 2, with the exception of verapamil, are accessible to both the aqueous and lipid environment.

Structures of TMR-S and TMR-Se. Spatial relationships among hydrogen-bond donors and acceptors are important for binding of substrates and inhibitors to Pgp (*8*, *28*, *53*). Introduction of the larger chalcogen atoms S and Se into the xanthylium core might impact the planarity of the xanthylium core as well as distances between the hydrogen-bond accepting N atoms of the 3,6-diamino substituents and the heteroatom of the xanthylium core. X-ray crystal structures of R6G and R123 (Chart 1) have shown that the xanthylium ring is planar and that the N−N distance between the 3,6-diamino substituents is 10.0 Å and the N−O distance is 5.0 Å (*56*).

Crystals of TMR-S and TMR-Se were characterized by X-ray crystallography as shown in the Oak Ridge thermal ellipsoid plot (ORTEP) drawings of Figures 1 and 1S (Supporting Information), respectively. The xanthylium core of both molecules is planar, and the N1−N2 distances are 10.007 Å for TMR-S and 10.155 Å for TMR-Se, while the N−S and N−Se distances are approximately 5.04 and 5.13 Å, respectively. The N−N and N-heteroatom distances are quite similar to those of R6G and R123 (*56*) despite the long C−S (1.73 Å) and C−Se (1.88 Å) bonds in TMR-S and TMR-Se. Dihedral angles between the xanthylium plane and the 9-phenyl substituents are 68.9° for TMR-S and 86.9° for TMR-Se, which are similar to the dihedral angles of 63.3° and 88.0° observed for R6G and R123, respectively (*56*). The dimethylamino substituents at the 3- and 6-positions are also coplanar with the xanthylium core with considerable double-bond character to the C−N bonds to the ring.

Pgp ATPase Activity. We note that many of the thio- and selenoxanthylium analogues of Chart 2 have shown activity as photosensitizers (*43*, *44*). Consequently, all interactions of these derivatives with Pgp were conducted in the dark.

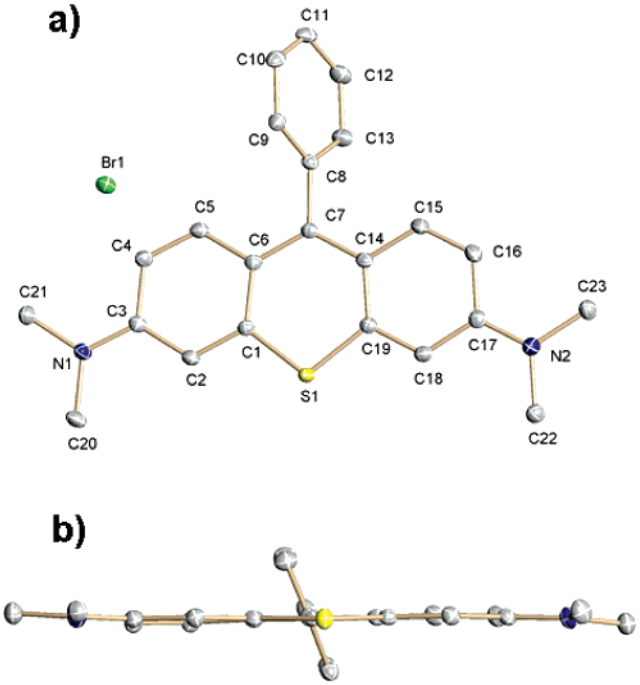

FIGURE 1: ORTEP plot and label scheme for TMR-S. Displacement ellipsoids are drawn at the 50% probability level viewed (a) from the top and (b) edge down the S1−C7 axis. Hydrogen atoms are omitted for clarity.

We determined the K_M^D, the apparent Michaelis−Menten constant for the stimulating drug, the drug-induced stimulation of maximal ATPase activity (V_M^{ATP}) for TMR-S, TMR-Se, **1**−**22**, and the rhodamines TMR, R123, and R6G using lipid-activated, mouse MDR3 Cys-less Pgp (Table 1) (*51*). Mouse MDR3 Pgp is 87% identical to human MDR1 Pgp in sequence. Verapamil (VER) was also included as a control compound in Table 1. ATP hydrolysis was determined via a spectrophotometric-coupled assay, and K_M^D and V_M^{ATP} were determined using an activity-partitioning model as described earlier (*52*). In this model, P-glycoprotein partitions its activity between an uncoupled basal activity cycle and a coupled activity cycle depending upon drug concentration. Stock solutions of VER, rhoadamine, or TMR analogues were prepared in DMSO. Basal activity in the presence of DMSO alone (2 vol %, control samples performed in parallel) was routinely ∼0.40 (nmol/min)/μg (∼0.70 s^{-1}). Control VER-stimulated ATPase activity was routinely ∼4.2 (nmol/min)/μg (∼7.3 s^{-1}).

At higher drug concentrations, binding to a second allosteric site can inhibit drug-induced stimulation of Pgp ATPase activity (*13*, *52*). As shown in Figure 2 and in the ATPase stimulation figures found in the Supporting Information, our measurements were made below the inhibitory concentrations. Consequently, K_i for inhibition was assumed to be large (>1000 μM) and the [drug]/(K_i + [drug]) term becomes vanishingly small in eq 1 reducing to eq 2 (Materials and Methods). We find a variation of K_M^D of approximately 2 orders of magnitude for this set of analogues (from a K_M^D of 392 μM for **9** to a K_M^D of 4 μM for **21**) and V_M^{ATP} variation between 0.9 and 5.0 (nmol/min)/μg, which is somewhat larger than VER stimulation (generally considered relatively robust).

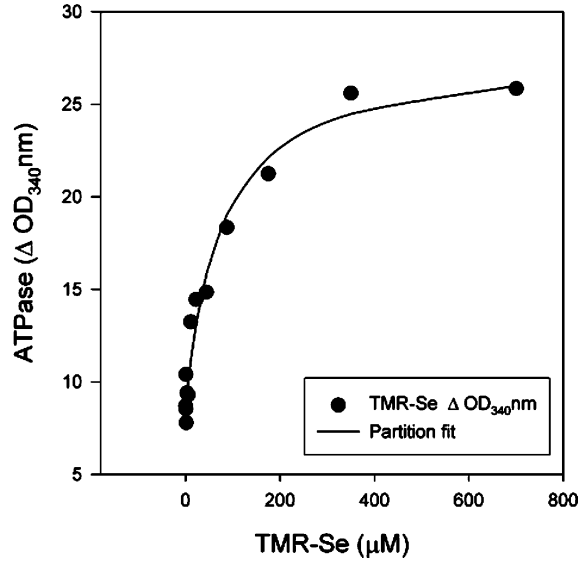

FIGURE 2: ATPase activity for various concentrations of TMR-Se. The line is the partition fit of the data to give K_M^D of 74 ± 19 μM and V_M^{ATP} of 0.93 ± 0.20 (nmol/min)/μg.

Thermodynamic analysis of ATP hydrolysis and drug transport has shown that stimulation of Pgp ATPase activity is strongly coupled to drug transport through a common, rate-limiting transition state, and that drugs transported at a higher rate require fewer conformational rearrangements to achieve the transition state (*13*). It follows that K_M^D for the stimulation of ATPase activity is directly related to binding for drug transport. The specificity constant, k_a(ATPase), for drug-induced stimulation of ATPase activity is defined by the ratio V_M^{ATP}/K_M^D. Values of k_a(ATPase) for TMR-S, TMR-Se, **1**−**22**, and the rhodamines TMR, R123, and R6G as well as their relative values, k_{rel}, which were determined with k_a-(ATPase) for TMR set at k_{rel} of 1.0, are also compiled in Table 1.

Rhodamine Stimulation of Pgp ATPase Activity. The rhodamine derivatives TMR, R123, and R6G have been previously examined (*40*) for their ability to stimulate ATPase activity in reconstituted Pgp and were evaluated in our study as control derivatives. Values of K_M^D and V_M^{ATP} are compiled in Table 1. Both R123 and TMR were similar with respect to K_M^D and V_M^{ATP}, while R6G was roughly 3-fold more stimulating.

In the earlier study (*40*), Pgp ATPase stimulation with TMR, R6G, and R123 was measured with Pgp as proteoliposomes (without detergent), while Pgp in our study was activated with *E. coli* lipids (with detergent). Levels of stimulation are quite different in the two studies (<1-fold above basal in ref *40*, >6-fold above basal in our study), which suggests that absolute comparisons are inappropriate. Despite this difference, qualitative results are similar. Our results indicate an order for V_M^{ATP} of R6G > R123 > TMR, which is qualitatively identical to the earlier study in which values of V_M^{ATP} were on the order R6G > TMR ≈ R123 (*40*). Values of K_M^D also followed similar trends where R6G < TMR < R123 in the earlier study (*40*), which is identical to our observed order of R6G < TMR < R123 (Table 1).

TMR-Analogue Stimulation of Pgp ATPase Activity. The first focus of the library of TMR analogues was the impact of heteroatom substitution on ATPase stimulation. Substitution of S and Se for O in the TMR analogues of Chart 2 had little impact on values of K_M^D if one compares TMR, TMR-S, and TMR-Se as one series (64−74 μM), compounds **3**−**5** as a second series (7−28 μM), and compounds **6**−**8** as a third series (26−54 μM, Table 1). The one exception is compound **3** with K_M^D of 7 μM, while **4** and **5** have K_M^D's of 20 and 28 μM, respectively. In general, Se-containing derivatives appear to have higher values of K_M^D relative to O- and S-containing derivatives. Within these same series, heteroatom substitution had little impact on values of V_M^{ATP}, with the exception that ATPase stimulation is somewhat more robust for **6** relative to **7** and **8** (Table 1).

Another focus of the library of TMR analogues in Chart 2 was the impact of substituent size in the 9-position. A comparison of the phenyl substituent in TMR-S with the 1-naphthyl substituent in **14** indicated a negligible change in K_M^D with one-third of the maximal stimulation of ATPase with the larger substituent (Table 1). Replacement of the phenyl substituents of TMR-S and TMR-Se with 2-thienyl substituents in **19** and **20** gave derivatives that showed little stimulation of ATPase activity at concentrations up to 500 μM. A decrease in the size of the 9-substituent from phenyl in TMR-S to an ethyl group in **16** reduced K_M^D by 25% and gave a 60% increase in V_M^{ATP} leading to a doubling of ATPase specificity (Table 1).

The major focus of the library of TMR analogues in Chart 2 was the impact of the number and placement of hydrogen-bond-accepting groups. Both of the 3,6-dimethylamino substituents appear to be important for TMR derivatives to stimulate ATPase activity in Pgp. The 3-dimethylaminothioxanthylium derivative **13** showed no stimulation of ATPase activity at concentrations up to 500 μM. In contrast, its 3,6-bis(dimethylamino)thioxanthylium analogue **7** (k_{rel} of 2.2) gave a K_M^D of 26 μM and V_M^{ATP} of 2.0 (nmol/min)/μg.

The introduction of hydrogen-bond acceptors in the 9-aryl substituents gave a 200-fold range of values of k_a(ATPase) as shown in Table 1. The introduction of a 4-methoxyphenyl group gave no change in K_M^D for both **1** and **2** relative to TMR-S and TMR-Se, respectively, and, for selenoxanthylium derivative **2**, a 70% increase in V_M^{ATP}. In contrast, 3-methoxyphenyl substituents gave large reductions in K_M^D for derivatives **3**−**5** (K_M^D of 7, 20, and 28 μM, respectively), although ATPase stimulation was increased only for **5** relative to TMR-Se (V_M^{ATP} of 2.5 and 0.9 (nmol/min)/μg, respectively). Interestingly, the introduction of 3,4-dimethoxyphenyl substituents showed little synergy, and values of K_M^D for **6**−**8** were higher than for the corresponding analogue in the series **3**−**5** (although less than **1** and **2**), although V_M^{ATP} was somewhat higher for **6** relative to **3** (Table 1).

The introduction of 3- or 4-dimethylaminophenyl substituents in TMR-S gave an increase in K_M^D and a decrease in ATPase stimulation (Table 1) with values of k_a(ATPase) of only 10% and 40% for **9** and **10**, respectively, relative to that of TMR-S. In contrast, the introduction of 3- or 4-aminophenyl substituents gave a reduction in K_M^D (20 μM for **11**, 18 μM for **12**) relative to TMR-S, and even though both **11** and **12** induced poorer ATPase activity than TMR-S, values of k_a(ATPase) were 2- and 3-fold larger, respectively, than for TMR-S. Interestingly, placing the hydrogen-bond acceptor in the 3-position gave better specificity than placing the hydrogen-bond acceptor in the 4-position, as was observed with 3-methoxy- and 4-methoxyphenyl derivatives.

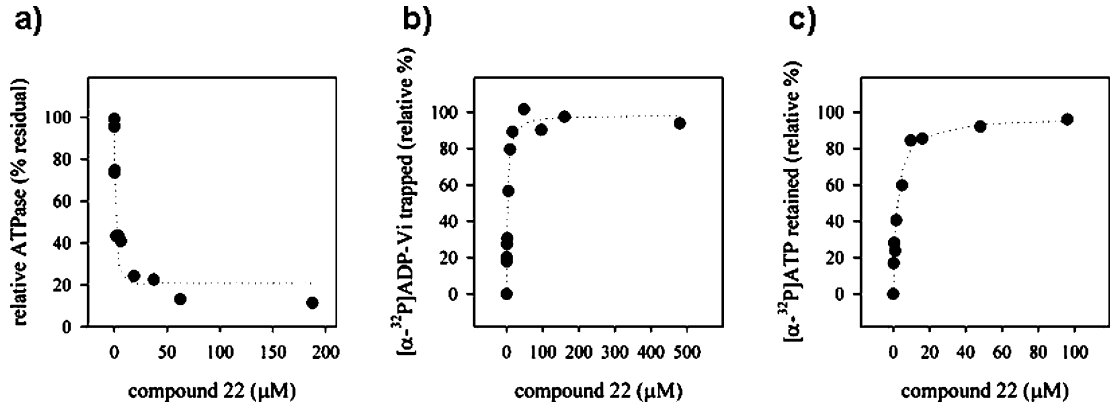

FIGURE 3: Effect of compound **22** on Pgp catalytic site. (a) Effect of **22** on ADP−Vi trapping in the absence of hydrolysis; (b) effect of **22** on [α-^{32}P]ADP−Vi trapping after hydrolysis and phosphate release; (c) effect of **22** on [α-^{32}P]ATP occlusion by E552A/E1197A double catalytic carboxylate mutant Pgp. The data represent the average of two experiments performed with two different Pgp preparations (for both wild-type and E552A/E1197A mutant). Data showed excellent agreement with less than 10% standard error in each case. For the experiments with radioactivity, 100% on the scale represents a stoichiometry of 1:1. Detailed descriptions of methods are provided in Materials and Methods.

The differences in activity between hydrogen-bond acceptors in the 3- and 4-positions of the 9-phenyl substituent suggest that small changes in atomic distances in a single substituent can have large influences on catalytic activity with TMR-related structures. The phenoxypropyl group in derivatives **17** and **18** places the hydrogen-bond acceptor the same number of bonds away as in the 3-methoxyphenyl substituent in derivatives **3**−**5**, but the 3-phenoxypropyl substituent has much greater conformational mobility. Both **17** and **18** were more effective than TMR with respect to k_a(ATPase). In comparing the thioxanthylium analogues **4** and **18**, values of V_M^{ATP} are comparable and somewhat larger than the ATPase stimulation observed with **3**. However, K_M^D is significantly smaller for **18** relative to **4**, and k_a(ATPase) is greater for **18** (k_{rel} of 8.8) relative to **4** (k_{rel} of 3.4) and is comparable for **18** and **3** (k_{rel} of 9.1).

In all of the compounds examined, the proper location of a single alkoxy group as a hydrogen-bond acceptor was able to stimulate ATPase activity at lower concentrations of drug relative to TMR, TMR-S, and TMR-Se. The 2-thienyl substituent in **19** and **20** gave derivatives that gave little stimulation of ATPase activity, and any enhancement observed upon the introduction of a hydrogen-bond acceptor on this scaffold should primarily reflect substituent effects. The 2-thienyl carboxamide derivatives **21** and **22** were prepared to introduce a hydrogen-bond acceptor at approximately the same location as those found in **3**−**5**, **17**, and **18**. Both **21** (k_{rel} of 30) and **22** (k_{rel} of 25) gave surprisingly robust stimulation of ATPase activity (V_M^{ATP} of 4.0 and 5.0 (nmol/min)/μg, respectively) with the lowest values of K_M^D observed in this study (4 and 6 μM for **21** and **22**, respectively).

The >200-fold differences observed in k_a(ATPase) among the library of TMR derivatives described in Chart 2 allow structure−activity relationships to be examined with much greater sensitivity than has been possible in studies with commercially available rhodamines (*40*). As described below, our focused library allows us to address some binding requirements at the "R" site of Pgp and determine potent stimulators of ATP hydrolysis for Pgp.

Enhancement of ADP−Vi Trapping or ATP Occlusion by Drugs. Pgp ATPase activity is slowly inhibited by the combination of ADP and vanadate anion (Vi) (*20*). Drugs that bind (stimulate) to Pgp greatly accelerate the rate of inhibition of Pgp by ADP and Vi. This effect was attributed to stimulation of a slow isomerization step following ADP binding that allowed the ADP·Vi complex to mimic closely the transition state of hydrolysis. In this scenario, the effect of drugs was pronounced, since they allow Pgp to overcome a large activation energy barrier associated with reaching the transition state from the reverse direction of the normal hydrolysis reaction. It was argued that the slow isomerization step involved the formation of a properly coordinated NBD dimer where ADP·Vi is tenaciously trapped within the catalytic site (*20*). Importantly, the concentration of VER required to stimulate Pgp ATPase activity was similar to the amount required to stabilize the ADP·Vi trapped conformation. This is consistent with the proposal that the primary effect of drug on Pgp catalysis is to stabilize a transition state-like conformation.

If correlation between drug activation of ATPase and ADP·Vi trapping were a general phenomenon, differences in specificity conferred by the TMR analogues (see k_{rel}, Table 1) would be expected to correlate with their ability to facilitate ADP·Vi trapping. To test whether k_{rel} values correlate with stabilization of ADP·Vi trapping, two well-established complementary assays were performed. The first assay measures ADP·Vi trapping from the reverse direction of the normal catalytic pathway and does not involve hydrolysis. Lipid-activated wild-type MDR3 Pgp (*57*) was incubated with ADP, Vi, and various concentrations of VER, TMR-S, or **22**. TMR-S and **22** were chosen since they display significantly different K_M^D values (70 versus 6 μM, respectively), and VER was a control. Following passage through centrifuge columns to remove free ADP, Vi, and drug, residual ATPase activity was determined for the eluted samples. As shown in Figure 3A and data in the Supporting Information, loss of ATPase activity as a function of drug concentration was fit to an equation with a single exponential from which values of IC_{50}, the concentration of drug to give 50% inhibition of residual ATPase activity, were extracted. The IC_{50} for VER was measured at 7.9 ± 1.6 μM (Figure 3S, Supporting Information), which is not significantly different than its value for K_M^D of 20 ± 4 μM. The IC_{50} for

TMR-S was measured at 100 ± 19 μM, which is similar to its value for K_M^D of 70 ± 15 μM (Figure 4S, Supporting Information). Importantly, analogue **22**, which conferred a robust ATPase stimulation ($V_M^{ATP} \sim 5$ (nmol/min)/μg and K_M^D of 6 ± 1 μM), displayed an IC_{50} of 2.4 ± 0.7 μM.

A second complementary assay was next employed to test the correlation of drug stimulation of ATPase and ADP·Vi trapping. In this case, hydrolysis is permitted (Vi binds after the release of phosphate, Pi), and trapping is directly ascertained by quantitation of [α-^{32}P]ADP·Vi retained by Pgp after passage through a centrifuge column. Similar relative correlations were found. Apparent K_M^D values for stimulation of [α-^{32}P]ADP·Vi trapping were 2.7 ± 0.5 μM for **22** (Figure 3B), 19.2 ± 3 μM for TMR-S (Figure 4S, Supporting Information), and 1.0 ± 0.2 μM for VER (Figure 3S, Supporting Information).

Recently, by analysis of a "catalytic carboxylate" double mutant Pgp (MDR3 E552A/E1197A), it was argued that, in the normal catalytic pathway, drugs promote the formation of an NBD dimer where ATP is occluded and poised for hydrolysis at a single site (*23*, *24*). We next examined whether effects noted by K_M^D for ATPase stimulation and ADP·Vi trapping described above would display a similar effect on ATP occlusion by E552A/E1197A mutant Pgp. This was indeed the case. Similar experiments using retention of [α-^{32}P]ATP through centrifuge columns revealed apparent K_M^D values for stimulation of [α-^{32}P]ATP occlusion to be 2.1 ± 0.4 μM for **22** (Figure 3C), 10.5 ± 2.4 μM for TMR-S (Figure 4S, Supporting Information), and 1.3 ± 0.3 μM for VER (Figure 3S, Supporting Information).

DISCUSSION

Structure−Activity Studies of the Stimulation of ATPase Activity. The basic structure of TMR consists of three hydrogen-bond acceptors in the form of the two dimethylamino nitrogen atoms at the 3- and 6-positions of the xanthylium core as well as the xanthylium oxygen atom. The 9-phenyl substituent serves as a hydrophobic group and/or as a π-electron donor. Seelig discusses the importance of tight-binding between a substrate and its transporter and the importance both of π-electron interactions with a cation and hydrogen-bonding interactions between a substrate and its transporter (*8*, *58*, *59*). For hydrogen-bonding interactions with the substrate, these can be defined as so-called Type I and Type II hydrogen bond-acceptor units, which interact with a high density of hydrogen-bond donor groups in the transmembrane sequences of Pgp. The Type I units have two hydrogen bond-acceptor atoms located 2.5 ± 0.5 Å apart (such as the two O atoms of an ester or carboxylic acid, the N and O atoms of an amide, or the two O atoms of an *ortho*-dimethoxyphenyl substituent) while the Type II units have two hydrogen bond-acceptor atoms located 4.6 ± 0.6 Å apart (such as the amino N atom and the xanthylium O atom of TMR or another rhodamine derivative). The N−O distances in TMR are roughly 5.0 Å (*56*), which constitute two Seelig Type II units in the basic TMR structure. The substitution of S and Se for O in the TMR core has very little impact on the N−chalcogen-atom distances, which are 5.04 in TMR-S and 5.13 Å in TMR-Se. The order of hydrogen bond-acceptor strength is O > S > Se, and relative values of k_a(ATPase) reflect this with k_{rel} of 1.0 for TMR, 1.0 for TMR-S, and 0.4 for TMR-Se. Replacing the phenyl substituent of TMR with the larger 1-naphthyl substituent in **14** and **15** gave a reduction in k_a(ATPase) for **14** (40% of TMR-S)and no observable ATPase stimulation with **15**, while replacing the phenyl substituent of TMR with a smaller ethyl substituent in **16** gave a doubling of k_a(ATPase). While π-interactions with a cation may be important, effective drug transport at the "R" drug-binding pocket (as measured by stimulation of ATPase activity) appears to have steric constraints, as well, at the 9-position of the TMR structure. Both N atoms in the 3,6-dimethylamino substituents appear to be critical to stimulate ATPase activity. Derivative **13**, which has only one dimethylamino substituent on the xanthylium core (and, thus, only one Seelig Type II unit) shows no stimulation of ATPase activity at concentrations as high as 500 μM.

Values of k_a(ATPase) can be further enhanced by the incorporation of additional hydrogen-bond acceptors at appropriate places. The introduction of 4-methoxy substituents in derivatives **1** and **2** had a modest impact on k_a(ATPase) relative to TMR-S and TMR-Se, respectively, but the introduction of 3-methoxyphenyl substituents in **3**−**5** gave 3- to 9-fold increases in k_a(ATPase) relative to TMR, TMR-S, and TMR-Se, respectively.

As shown in Figures 1 and 1S (Supporting Information), the 9-phenyl substituents are nearly orthogonal to the plane of the xanthylium ring in TMR-S and TMR-Se as was observed with R6G and R123 (*56*). Interactions of the *ortho*-hydrogen atoms of the phenyl group with the *peri*-hydrogen atoms of the xanthylium core prevent these two groups from being coplanar. In addition, the TMR scaffold is a fairly rigid structure. Substituents added to the 4-position of the phenyl ring as found in derivatives such as **1** and **2** (4-methoxy), **9** (4-dimethylamino), and **11** (4-amino) are "fixed" in space with little conformational mobility. Substituents added to the 3-position of the phenyl ring such as **3**−**5** (3-methoxy), **10** (3-dimethylamino), and **12** (3-amino) have more mobility in space, but will be confined to the arc of minimal steric interactions between the phenyl ring and xanthylium core.

The introduction of a Seelig Type I unit in the form of the 3,4-dimethoxyphenyl substituent gave values of k_a(ATPase) that were somewhere between the activity of the 4-methoxy derivatives **1** and **2** and the 3-methoxyphenyl derivatives **3**−**5**. No synergy was observed by adding the second group. One might suggest that the 3,4-dimethoxyphenyl substituent has unfavorable steric interactions or that the rigid nature of the xanthylium core and the lack of spatial mobility in the 4-methoxy substituent may prevent this Seelig Type I unit from achieving a proper orientation.

The 9-(4-dimethylaminophenyl) substituent in **9** gave a 7-fold reduction in k_a(ATPase) relative to **1**, while the 9-(3-dimethylaminophenyl) substituent in **10** gave an 8.5-fold reduction in k_a(ATPase) relative to **4**. Even though the dimethylamino substituent should be a better hydrogen-bond acceptor than the methoxy substituent, the greatly reduced specificity/activity observed with **9** and **10** again suggests that steric interactions are important in the 9-substituents with respect to ATPase stimulation.

Since alkyl groups are tolerated at the 9-position as demonstrated by the enhanced activity of the 9-ethyl derivative **16**, the 9-(3-phenoxypropyl) substituent was evaluated as a flexible tether for the hydrogen-bond acceptor. Even though increased entropic demands with a flexible tether may

reduce ΔG for binding, the enthalpic gains lead to a 2.5-fold increase in k(ATPase) for **18** relative to **4**, primarily by lowering K_M^D.

The enhanced activity with a conformationally mobile hydrogen-bond acceptor in the 9-position of **17** and **18** reaffirmed that the Seelig Type I acceptors (the 3,4-dimethoxyphenyl group) in **6**−**8** might not be capable of adopting a favorable orientation. Although **19** and **20** with 9-(2-thienyl) substituents show little ATPase stimulation at concentrations up to 500 μM, the introduction of the 5-*N*,*N*-diethylcarboxamide group on the thienyl substituent gave the two most active stimulators of ATPase of this study (≈25−30-fold increase in k_a(ATPase) relative to TMR). In these derivatives, the carboxamide group (a Seelig Type I group) can be oriented in roughly the same place as the methoxy group of the 3-methoxyphenyl substituent in **3**−**5**. While the 2-thienyl-5-carboxamide group was chosen for ease of synthesis, other 3-carboxamide-substituted phenyl derivatives may behave similarly.

The library of TMR derivatives described here validates the presence of the "R" binding site in Pgp first described by Shapiro and Ling (*25*, *26*) and also illustrates the importance of hydrogen bond-accepting groups in promoting tight binding of the substrate with the transporter. In TMR-related molecules (including rhodamine derivatives) that bind to the "R" site and stimulate ATPase activity, both hydrogen bond-accepting amino groups at the 3- and 6-positions of a chalcogenoxanthylium core are critical structural features. While a 9-phenyl substituent in TMR and TMR-S is sufficient to stimulate ATPase activity with increasing concentrations of drug, enhanced binding to the "R" site and enhanced stimulation of ATPase relative to TMR are observed if a hydrogen bond-accepting group is placed roughly 5−6 Å away from the 9-position of the xanthylium core and even greater binding is observed if the hydrogen bond-accepting group has conformational mobility to be out of the xanthylium plane. Enhanced stimulation of Pgp ATPase activity relative to TMR is also observed if the 9-phenyl substituent is replaced with a smaller alkyl group.

The TMR analogues of Chart 2 interact with Pgp to give a >200-fold range of k_a(ATPase) resulting from fairly minor structural changes and an even greater range if one considers the "inactive" compounds. One can reasonably ask the question whether all of these structures bind to the same site and whether the various structures follow the same mechanistic path for coupling of ATP binding and hydrolysis with drug export. Below, we discuss in much greater detail the coupling of ATP binding and hydrolysis with the apparent K_M^D for TMR-S and compound **22**, which differ by 26-fold in k_a(ATPase).

Binding of TMR Analogues and the Transition State for ATP-Hydrolysis and Implications for Mechanism. Thermodynamic analysis of the transition state of Pgp has shown that ATP hydrolysis and transport are coupled (*13*), but the communicative mechanism between the TMDs and the NBDs that allows coupling between domains is not well-understood. A heuristic example illustrating the molecular basis for coupling is found in crystallographic studies of the nitrogenases where ATP hydrolysis is coupled to an electron-transfer reaction (*60*, *61*). In this case, it was demonstrated through crystal structures of intermediates that effective coupling is contingent upon shared conformational transitions between the two processes. Recent data from the Gadsby lab demonstrated that ABC proteins likely behave similarly (*62*, *63*). In this case, coordinated coupled conformational changes were measured in the intact CFTR channel (an ABC protein homologue of Pgp). When ATP hydrolysis and associated NBD dimerization were prevented or probed by mutation, patch-clamp recordings revealed that the channel remained open for greatly extended periods if NBD dimerization was stabilized. This clearly illustrated that tight ATP binding at the NBDs elicited a coordinated change at the TMDs, that is, channel opening. By analogy, in the case of Pgp, the chemical nature of the "drug" should dictate the efficiency of drug efflux by effective communication to the distal NBDs and vice versa. That is, drug binding and efflux must elicit conformational transitions that productively influence distal NBD ATPase cycles. Reciprocally, as the ATP is bound and hydrolyzed, and Pi and/or ADP is released, the availability of the drug binding site and/or trajectory must be influenced by coordinated shared conformational transitions.

We have demonstrated that the "R"-site, drug-dependent, trigger mechanism for hydrolysis activation and coupling to the distant NBDs can be systematically probed by variation of a scaffold. Our designed library of TMR-related structures has produced a range of K_M^D values for binding in the TMDs that stimulate the hydrolysis of ATP in the NBDs. A strong correlation between the concentrations required to stimulate ATPase activity (turnover) and to promote ADP−Vi trapping (forming the closed conformation), K_M^D and IC_{50}, respectively, was observed for VER, TMR-S, and **22**. Similarly, K_M^D correlated with the concentration of drug required to enhance the rate of ADP−Vi trapping when hydrolysis is permitted (starting with ATP) as well as with ATP occlusion when hydrolysis is attenuated (with E552A/E1197A mutant protein). Thus, by employing the set of compounds described herein, we have demonstrated that discrete effects on catalytic efficiency correlate well with discrete effects at the ATP catalytic site. It follows that the shared coupled conformation involves drug binding to trigger NBD closure and asymmetric involvement of catalytic site residues to initiate hydrolysis.

These data are consistent with mounting evidence that a key conformational transition associated with coupling, and common to the acceleration of each of these activities, is the formation of an asymmetric closed NBD dimer intermediate where ATP is occluded at a single site and catalytic site residues are properly engaged for hydrolysis. Structural data of full-length homologous ABC transport proteins clearly indicate that an intracytoplasmic loop/extension of TMD helices could communicate drug binding to the NBDs and vice versa (*16*−*19*). Moreover, a recent structure of the full-length lipid flippase MsbA from *Salmonella* demonstrates a lipid substrate-bound form that is asymmetric with ADP−Vi retained tightly at a single NBD (*18*). Electron microscopy studies indicate that ATP binding and/or hydrolysis elicits conformational changes in the TMDs of Pgp that appear to facilitate drug transport (*64*). Since a structure of Pgp is unavailable presently, our data will provide testable predictions with regard to structural models of Pgp and the molecular details of coupling and drug trajectory.

Accumulated data indicate that Pgp binds drugs from the inner (cytoplasmic) leaflet of the plasma membrane (vacuum cleaner model) (*65*, *66*). Next, there are two possible

trajectories that have been proposed, which involve movement of TMD helices. In the flippase mechanism, coupled conformational changes in the protein will elicit movement of the drug to the outer leaflet of the membrane with concomitant reduced affinity and export (*67*). In this case, the need for an aqueous vestibule as an intermediate may be obviated. In contrast, other schemes involve conformational changes (likely rotation of TMD helices) in which the drug moves from the high-affinity site to an aqueous-accessible lower affinity site, whereby efflux occurs by diffusion from the chamber (*28*, *38*, *68*). It has been hypothesized that the drug must pass through "gates" comprised of TMD helices. The nature of drug−Pgp interactions at the "R" site required for coupling described herein may shed insight on the trajectory of drugs during the catalytic cycle and may discriminate between these models as structural data become available.

Drug stimulation of ATPase activity and coupling to the ATP catalytic site appear tunable (not a simple all-or-nothing relationship; see k_{rel} values, Table 1) depending upon the nature of the molecular interactions. Using a focused library of TMR analogues to probe a biological process, our observations extend the notion that π-interactions and hydrogen bond-acceptor availability are critical criteria for evaluating Pgp−drug interactions as well as eliciting the conformational transitions that facilitate coupling. Another key tenet is that, for coupling to be effective, the shared conformations must be productive and not dissipate, since this will lead to futile cycles. One possible outcome that a continued analysis may permit is for drug binding to be competitive, yet nonproductive, causing a futile or aborted cycle. In this case, if tight binding is allowed without triggering hydrolysis or conformational transitions necessary for drug movement, and these effects can be predicted, it may be possible to design more efficient TMR-related inhibitors of Pgp efflux.

ACKNOWLEDGMENT

The authors gratefully acknowledge Alan Senior for encouragement and support from his grant to study Pgp mechanism (GM50156), Sarah Lockwood for excellent technical assistance, Matt Disney for the use of his space for experiments with radioactivity, and Bruce Holm, Director of the NYS Center for Excellence in Bioinformatics and Life Sciences, for space and instrumental resources.

SUPPORTING INFORMATION AVAILABLE

Figure 1S (molecular structure of TMR-Se), Figure 2S (fold stimulation of ATPase activity above basal for various concentrations of TMR analogues), Figure 3S (effect of Verapamil on ATP catalytic site), Figure 4S (effect of TMR-S on ATP catalytic site), Table 1S (crystallographic data for TMR-S and TMR-Se), Table 2S (atomic coordinates and equivalent isotropic displacement parameters for TMR-S), Table 3S (anisotropic displacement parameters for TMR-S), Table 4S (bond lengths and angles for TMR-S), Table 5S (atomic coordinates and equivalent isotropic displacement parameters for TMR-Se), Table 6S (anisotropic displacement parameters for TMR-Se), and Table 7S (bond lengths and angles for TMR-Se). This material is available free of charge via the Internet at http://pubs.acs.org.

REFERENCES

1. Ambudkar, S. V., Dey, S., Hrycyna, C. A., Ramachandra, M., Pastan, I., and Gottesman, M. M. (1999) Biochemical, Cellular, and Pharmacological Aspects of the Multidrug Transporter, *Annu. Rev. Pharmacol. Toxicol. 39*, 361−368.
2. Gottesman, M. M. and Ling, V. (2006) The Molecular Basis of Multidrug Resistance in Cancer: The Early Years of P-glycoprotein Research, *FEBS Lett. 580*, 998−1009.
3. Gottesman, M. M., Fojo, T., and Bates, S. E. (2002) Multidrug Resistance in Cancer: Role of ATP-dependent Transporters, *Nat. Rev. Cancer 2*, 48−58.
4. Owen, A, Chandler, B., and Back, D. J. (2005) The Implication of P-glycoprotein in HIV: Friend or Foe? *Fundam. Clin. Pharmacol. 19*, 283−296.
5. Van Bambeke, F., Balzi, E., and Tulkens, P. M. (2000) Antibiotic Efflux Pumps, *Biochem. Pharmacol. 60*, 457−470.
6. Borst, P. M., and Ouellette, M. (1995) New Mechanisms of Drug Resistance in Parasitic Protozoa, *Annu. Rev. Microbiol. 49*, 427−460.
7. Wolfger, H., Mamnun, Y. M., and Kuchler, K. (2001) Fungal ABC Proteins: Pleiotropic Drug Resistance, Stress Response and Cellular Detoxification, *Res. Microbiol. 152*, 375−389.
8. Seelig, A., and Gatlik-Landwojtowicz, E. (2005) Inhibitors of Multidrug Efflux Transporters: Their Membrane and Protein Interactions, *Mini-Rev. Med. Chem. 5*, 135−151.
9. Szakács, G., Annereau, J., Lababidi, S., Shankavaram, U., Arciello, A., Bussey, K. J., Reinhold, W., Guo, Y., Kruh, G. D., Reimers, M., Weinstein, J. N., and Gottesman, M. M. (2004) Predicting Drug Sensitivity and Resistance: Profiling ABC Transporter Genes in Cancer Cells. *Cancer Cell 6*, 129−137.
10. Senior, A. E., Al-Shawi, M. K., and Urbatsch, I. L. (1995) The Catalytic Cycle of P-glycoprotein, *FEBS Lett. 377*, 285−289.
11. Sauna, Z. E., and Ambudkar, S. V. (2001) Characterization of the Catalytic Cycle of ATP Hydrolysis by Human P-glycoprotein. The Two ATP Hydrolysis Events in a Single Catalytic Cycle Are Kinetically Similar but Affect Different Functional Outcomes, *J. Biol. Chem. 276*, 11653−11661.
12. Higgins, C. F., and Linton, K. J. (2004) The ATP Switch Model for ABC Transporters, *Nat. Struct. Mol. Biol. 11*, 918−926.
13. Al-Shawi, M. K., Polar, M. K., Omote, H., and Figler, R. A. (2003) Transition State Analysis of the Coupling of Drug Transport to ATP Hydrolysis by P-glycoprotein, *J. Biol. Chem. 278*, 52629−52640.
14. Rosenberg, M. F., Callaghan, R., Modok, S., Higgins, C. F., and Ford, R. C. (2005) Three-dimensional structure of P-glycoprotein: The Transmembrane Regions Adopt an Asymmetric Configuration in the Nucleotide-bound State, *J. Biol. Chem. 280*, 2857−2862.
15. Rosenberg, M. F., Kamis, A. B., Callaghan, R., Higgins, C. F., and Ford, R. C. (2003) Three-dimensional Structures of the Mammalian Multidrug Resistance P-glycoprotein Demonstrate Major Conformational Changes in the Transmembrane Domains upon Nucleotide Binding, *J. Biol. Chem. 278*, 8294−8299.
16. Smith, P. C., Karpowich, N., Millen, L., Moody, J. E., Rosen, J., Thomas, P. J., and Hunt, J. F. (2002) ATP Binding to the Motor Domain from an ABC Transporter Drives Formation of a Nucleotide Sandwich Dimer, *Mol. Cell 10*, 139−149.
17. Chen, J., Lu, G., Lin, J., Davidson, A. L., and Quiocho, F. A. (2003) A Tweezers-like Motion of the ATP Binding Cassette Dimer in an ABC Transport Cycle, *Mol. Cell 12*, 651−661.
18. Reyes, C. L., and Chang, G. (2005) Structure of the ABC Transporter MsbA in Complex with ADP·Vanadate and Lipopolysaccharide, *Science 308*, 1028−1031.
19. Locher, K. P., Lee, A. T., and Rees, D. C. (2002) The *E. coli* BtuCD Structure: A Framework for ABC Transporter Architecture and Mechanism, *Science 296*, 1091−1098.
20. Urbatsch, I. L., Tyndall, G. A., Tombline, G., and Senior, A. E. (2003) P-glycoprotein Catalytic Mechanism: Studies of the ADP−Vanadate Inhibited State, *J. Biol. Chem. 278*, 23171−23179.
21. Qu, Q., Russell, P. L., and Sharom, F. J. (2003) Stoichiometry and Affinity of Nucleotide Binding to P-Glycoprotein during the Catalytic Cycle, *Biochemistry 42*, 1170−1177.
22. Delannoy, S., Urbatsch, I. L., Tombline, G., Senior, A. E., and Vogel, P. D. (2005) Nucleotide Binding to the Multidrug Resistance P-Glycoprotein As Studied by ESR Spectroscopy, *Biochemistry 44*, 14010−14019.
23. Tombline, G., Bartholomew White, L., Muharemagic, A., and Senior, A. E. (2004) Combined Mutation of Catalytic Glutamate

Residues in the Two Nucleotide Binding Domains of P-glycoprotein Generates a Conformation that Binds ATP and ADP Tightly. *J. Biol. Chem. 279*, 31212−31220.
24. Tombline, G., Muharemagic, A., Bartholomew White, L., and Senior, A. E. (2005) Involvement of the "Occluded Nucleotide Conformation" of P-Glycoprotein in the Catalytic Pathway, *Biochemistry 45*, 12879−12886.
25. Shapiro, A. B., and Ling, V. (1997) Positively Cooperative Sites for Drug Transport by P-glycoprotein with Distinct Drug Specificities, *Eur. J. Biochem. 250*, 130−137.
26. Shapiro, A. B., and Ling, V. (1998) Stoichiometry of Rhodamine 123 Transport to ATP Hydrolysis by P-glycoprotein, *Eur. J. Biochem. 254*, 189−193.
27. Pajeva, I. K., and Wiese, M. (2002) Pharmacophore Model of Drugs Involved in P-Glycoprotein Multidrug Resistance: Explanation of Structural Variety (Hypothesis), *J. Med. Chem. 45*, 5671−5686.
28. Pajeva, I. K., Globisch, C., and Wiese, M. (2004) Structure−Function Relationships of Multidrug Resistance P-Glycoprotein, *J. Med. Chem. 47*, 2523−2533.
29. Pajeva, I. K., and Wiese, M. (2001) Human P-Glycoprotein Pseudoreceptor Modeling: 3D-QSAR Study on Thioxanthene Type Multidrug Resistance Modulators, *Quant. Struct.-Act. Relat. 20*, 130−138.
30. Martin, C., Higgins, C. F., and Callaghan, R. (2001) The Vinblastine Binding Site Adopts High- and Low-Affinity Conformations During a Transport cycle of P-Glycoprotein, *Biochemistry 40*, 15733−15742.
31. Omote, H., and Al-Shawi, M. K. (2002) A Novel Paramagnetic Resonance Approach to Determine the Mechanism of Drug Transport by P-glycoprotein, *J. Biol. Chem. 277*, 45688−45694.
32. Safa, A. R. (1998) Photoaffinity Labels for Characterizing Drug Interaction Sites of P-glycoprotein, *Methods Enzymol. 292*, 289−307.
33. Greenberger, L. M. (1998) Identification of Drug Interaction Sites in P-glycoprotein, *Methods Enzymol. 292*, 307−317.
34. Qu, Q., Chu, J. W., and Sharom, F. J. (2003) Transition Sate P-Glycoprotein Binds Drugs and Modulators with Unchanged Affinity, Suggesting a Concerted Transport Mechanism, *Biochemistry 42*, 1345−1353.
35. Loo, T. W., Bartlett, M. C., and Clarke, D. M. (2003) Methanethiosulfate Derivatives of Rhodamine and Verapamil Activate Human P-glycoprotein at Different Sites, *J. Biol. Chem. 278*, 50136−50141.
36. Loo, T. W., and Clarke, D. M. (2005) Do Drug Substrates Enter the Common Drug-Binding Pocket of P-glycoprotein through Gates? *Biochem. Biophys. Res. Commun. 329*, 419−422.
37. Szakács, G., Annereau, J., Lababidi, S., Shankavaram, U., Arciello, A., Bussey, K. J., Reinhold, W., Guo, Y., Kruh, G. D., Reimers, M., Weinstein, J. N., and Gottesman, M. M. (2004) Predicting Drug Sensitivity and Resistance: Profiling ABC Transporter Genes in Cancer Cells, *Cancer Cell 6*, 129−137.
38. Scala, S., Akhmed, N., Rao, U. S., Paull, K., Lan, L.-B., Dickstein, B., Lee, J.-S., Elgemeie, G. H., Stein, W. D., and Bates, S. E. (1997) P-glycoprotein Substrates and Antagonists Cluster into Two Distinct Groups, *Mol. Pharmacol. 51*, 1024−1033.
39. Lee, J. S., Paull, K., Alvarez, M., Hose, C., Monks, A., Grever, M., Fojo, A. T., and Bates, S. E. (1994) Rhodamine Efflux Patterns Predict P-glycoprotein Substrates in the National Cancer Institute Drug Screen, *Mol. Pharmacol. 46*, 627−638.
40. Eytan, G. D., Regev, R., Hurwitz, C. D., and Assaraf, Y. G. (1997) Efficiency of P-glycoprotein-Mediated Exclusion of Rhodamine Dyes from Multidrug-resistant Cells Is Determined by Their Passive Transmembrane Movement Rate, *Eur. J. Biochem. 248*, 104−112.
41. Lu, P., Liu, R., and Sharom, F. J. (2001) Drug Transport by Reconstituted P-glycoprotein in Proteoliposomes—Effect of Substrates and Modulators, and Dependence on Bilayer Phase State, *Eur. J. Biochem. 268*, 1687−1695.
42. Loetchutinat, C., Saengkhae, C., Marbeuf-Gueye, C., and Garnier-Suillerot, A. (2003) New Insights into the P-glycoprotein-Mediated Effluxes of Rhodamines, *Eur. J. Biochem. 270*, 476−485.
43. Gibson, S. L., Holt, J. J., Ye, M., Donnelly, D. J., Ohulchanskyy, T. Y., You, Y., and Detty, M. R. (2005) Structure−Activity Studies of Uptake and Phototoxicity with Heavy-Chalcogen Analogues of Tetramethylrosamine in Vitro in Chemosensitive and Multidrug-Resistant Cells, *Bioorg. Med. Chem. 13*, 6394−6403.
44. Wagner, S. J., Skripchenko, A., Donnelly, D. J., Ramaswamy, K., and Detty, M. R. (2005) Chalcogenoxanthylium Photosensitizers for the Photodynamic Purging of Blood-Borne Viral and Bacterial Pathogens, *Bioorg. Med. Chem. 13*, 5927−5935.
45. Ehrlich, P., and Benda, L. (1913) Action of Potassium Cyanide on Pyronine and Acridinium Dyes, *Ber. Dtsch. Chem. Ges. 48*, 1931−1943.
46. Del Valle, D. J.; Donnelly, D. J., Holt, J. J., and Detty, M. R. (2005) 2,7-Bis-*N*,*N*-dimethylaminochalcogeno-xanthen-9-ones via Electrophilic Cyclization with Phosphorus Oxychloride, *Organometallics 24*, 3807−3810.
47. Brennan, N. K., Donnelly, D. J., and Detty, M. R. (2003) Selenoxanthones via Directed Metalations in 2-Arylselenobenzamide Derivatives, *J. Org. Chem. 68*, 3344−3347.
48. Sangster, J. (1997) In *Octanol−Water Partition Coefficients: Fundamentals and Physical Chemistry* (Fogg, P. G. T., Ed.) John Wiley and Sons, New York.
49. Brüker Analytical X-ray Systems (2004) APEX2 and SAINT-Plus, Area Detector Control and Integration Software, Ver. 1.0-27. Brüker Analytical X-ray Systems, Madison, WI.
50. Brüker Analytical X-ray Systems (2003) SHELXTL, An Integrated System for Solving, Refining and Displaying Crystal Structures from Diffraction Data, Ver. 6.14, Brüker Analytical X-ray Systems, Madison, WI.
51. Tombline, G. L., Urbatsch, I. L., Virk, N., Muharemagic, A., White, B., and Senior, A. E. (2006) Expression, Purification, and Characterization of Cysteine-Free Mouse P-glycoprotein, *Arch. Biochem. Biophys. 445*, 124−128.
52. Omote, H., Fiegler, R. A., Polar, M. K., and Al-Shawi, M. K. (2004) Improved Energy Coupling of Human P-Glycoprotein by the Glycine 185 to Valine Mutation, *Biochemistry 43*, 3917−3928.
53. Globisch, C., Pajeva, I. K., and Wiese, M. (2006) Structure−Activity Relationships of a Series of Tarquadar Analogs as Multidrug Resistance Modulators, *Bioorg. Med. Chem. 14*, 1588−1598
54. Duvvuri, M., Gong, Y., Chatterji, D., and Krise, J. P. (2004) Weak Base Permeability Characteristics Influence the Intracellular Sequestration Site in the Multidrug-Resistant Human Leukemia Cell Line HL-60, *J. Biol. Chem. 279*, 32367−32372.
55. Litman, T., Zeuthen, T., Skovsgaard, T., and Stein, W. D. (1997) Structure−activity Relationships of P-glycoprotein-interacting Drugs: Kinetic Characterization of Their Effects on AATPase Activity, *Biochim. Biophys. Acta 1361*, 159−168.
56. Adhikesavalu, D. N., Mastropaolo, D., Camerman, A., and Camerman, N. (2001) Two Rhodamine Derivatives: 9-[2-(Ethoxycarbonyl)phenyl]-3,6-bis-(ethylamino)-2,7-dimethylxanthylium Chloride Monohydrate and 3,6-Diamino-9-[2-(methoxycarbonyl)-phenyl]xanthylium Chloride Trihydrate, *Acta Crystallogr., Sect. C: Cryst. Struct. Commun. 57*, 657−659.
57. Lerner-Marmarosh, N., Gimi, K., Urbatsch, I. L., Gros, P., and Senior, A. E. (1999) Large Scale Purification of Detergent-soluble P-glycoprotein from *Pichia pastoris* Cells and Characterization of Nucleotide Binding Properties of Wild-Type, Walker A, and Walker B Mutant Proteins, *J. Biol. Chem. 274*, 34711−34718.
58. Gatlik-Landwojtowicz, E., Aanismaa, P., and Seelig, A. (2006) Quantification and Characterization of P-glycoprotein−Substrate Interactions, *Biochemistry 45*, 3020−3032.
59. Seelig, A. (1998) A General Pattern for Substrate Recognition by P-glycoprotein, *Eur. J. Biochem. 251*, 252−261.
60. Rees, D. C., and Howard, J. B. (1999) Structural Bioenergetics and Energy Transduction Mechanisms, *J. Mol. Biol. 293*, 343−350.
61. Tezcan, F. A., Kaiser, J. T., Mustafi, D., Walton, M. Y., Howard, J. B., and Rees, D. C. (2005) Nitrogenase Complexes: Multiple Docking Sites for a Nucleotide Switch Protein, *Science 309*, 1377−1380.
62. Vergani, P., Lockless, S. W., Nairn, A. C., and Gadsby, D. C. (2005) CFTR Channel Openingby ATP-Driven Tight Dimerization of Its Nucleotide Binding Domains, *Nature 433*, 876−880.
63. Vergani, P., Nairn, A. C., and Gadsby, D. C. (2003) On the Mechanism of MgATP-Dependent Gating of CFTR Cl^- Channels, *J. Gen. Physiol. 120*, 17−36.
64. Callaghan, R., Ford, R. C., and Kerr, I. D. (2006) The Translocation Mechanism of P-glycoprotein, *FEBS Lett. 580*, 1056−1063.
65. Gottesman, M. M., and Pastan, I. (1993) Biochemistry of Multidrug Resistance Mediated by the Multidrug Transporter, *Annu. Rev. Biochem. 62*, 385−427.
66. Chen, Y., Pant, A. C., and Simon, S. M. (2001) P-glycoprotein Does Not Reduce Substrate Concentration from the Extracellular

Leaflet of the Plasma Membrane in Living Cells, *Cancer Res. 61*, 7763−7769.
67. Eckford, P. D. W., and Sharom, F. J. (2005) The Reconstituted P-glycoprotein Multidrug Transporter Is a Flippase for Glucosylceramide and Other Simple Glycosphingolipids, *Biochem. J. 389*, 517−526.
68. Loo, T. W., Bartlett, C., and Clarke, D. M. (2004) The Drug-Binding Pocket of the Human Multidrug Resistance P-Glycoprotein Is Accessible to the Aqueous Medium, *Biochemistry 43*, 12081−12089.

BI0603470